Available online at www.sciencedirect.com
ScienceDirect
Journal of Catalysis 251 (2007) 410–422
JOURNAL OF CATALYSIS
www.elsevier.com/locate/jcat

Highly selective CO methanation catalysts for the purification of hydrogen-rich gas mixtures

M. Krämer [a], M. Duisberg [b], K. Stöwe [a], W.F. Maier [a,*]

[a] *Lehrstuhl für Technische Chemie, Universität des Saarlandes, Gebäude C 4.2, 66123 Saarbrücken, Germany*
[b] *Umicore AG & Co. KG, Rodenbacher Chaussee 4, 63403 Hanau, Germany*

Received 29 March 2007; revised 13 July 2007; accepted 31 July 2007

Abstract

High-throughput techniques based on emissivity-corrected infrared thermography (ecIRT) were used in the discovery and optimization of new catalysts for the purification of hydrogen-rich gas reformates by means of CO methanation. The application of an appropriate sequence of test gases in the high-throughput experiment (HTE) enabled us to screen for activity as well as selectivity. From literature and prescreening of about 2000 samples of highly diverse mixed oxides, we selected suitable elements for more detailed studies in the first generation. Among these 1000 samples, various doped Ni oxides proved most promising and were selected as leads for the subsequent evolutionary optimization based on selection and variation. Rapid optimization was achieved during three catalyst generations. The improvement in the catalysts in terms of CO activity and selectivity was confirmed at various stages during the developing process by conventional gas-phase experiments. Compared with a typical industrial methanation catalyst (Ru/TiO_2), the $Re_2Y_9Ni_{89}O_x$ and $Ti_8Hf_9Ni_{83}O_x$ investigated here exhibit unique catalytic performances with respect to activity and selectivity, reducing or eliminating the problems of hydrogen loss by CO_2 methanation. Strong evidence for good stability of the best catalysts was obtained by long-term HT screening for about 100 h. Characterization of selected materials is provided.

Keywords: Methanation; CO removal; High-throughput experimentation; Combinatorial chemistry; Nickel catalyst; Sol–gel

1. Introduction

The proton-exchange membrane fuel cell is considered to play an important role in the future energy generation for mobile applications due to its high power density and zero emission and for stationary applications due to the generation of electricity and heat. However, it relies on hydrogen as fuel, and the use of liquid or compressed hydrogen carries several disadvantages with respect to supply, handling, and storage. The onsite production of hydrogen from either high-energy liquid fuels or natural gas provides a promising alternative, yielding a hydrogen-rich gas mixture that contains considerable amounts of H_2O, CO_2, and CO [1,2]. Hindering the anode electrokinetics, the amount of CO must be reduced from ∼1 vol% in the reformate to <100 ppm in an additional purification step [3].

Various approaches to reducing the CO content have been discussed in the literature. Membrane separation processes based on the diffusion of hydrogen through a Pd–Ag membrane can guarantee effective separation [4]. On the other hand, high costs of the membrane and the exigency of a high-pressure differential between both sides of the membrane cast this approach into doubt for industrial applications. The preferential oxidation of CO to CO_2 is the widely accepted method of choice [1,2]. Promising catalysts include supported Au nanoparticles [5], Cu–Ce mixed oxides [6], and the combinatorially discovered Mn–Co mixed oxides [7]. Nevertheless, complete removal of CO still requires high temperatures, and with the presently available catalysts, the undesired conversion of hydrogen to water cannot be avoided. Furthermore, an injecting system controlling the accurate addition of air causes additional complications. A promising alternative is the direct methanation of the remaining CO into CH_4 and H_2O. The effective removal of CO in reformate atmosphere has already been demonstrated by different authors [8–12]. Typical methanation catalysts rest

* Corresponding author. Fax: +49 (0) 681 302 2343.
E-mail address: w.f.maier@mx.uni-saarland.de (W.F. Maier).

0021-9517/$ – see front matter
doi:10.1016/j.jcat.2007.07.030

on metals of Group VIII, on Mo or on Ag, often containing expensive noble metals [13]. Advantages of this approach include the fact that no additional gas component is needed, and the CH_4 produced does not affect the fuel cell and can be used as burner fuel to heat the steam reformer. The amount of hydrogen consumed during the reaction with CO is negligible, due to the low CO content. The problem is the simultaneous methanation of CO_2, which consumes 4 mol of H_2 per mol of CO_2, amplified by the high CO_2 content in the reformate. State-of-the-art catalysts selectively convert CO until at high conversion, the methanation of CO_2 starts to dominate. Process requirements are that hydrogen consumption occurs only through CO methanation, with no additional loss by CO_2 reduction. This calls for catalysts that effectively reduce CO in a temperature range in which CO_2 does not react.

Consequently, in this study we attempted to discover new catalysts with low noble metal content and high selectivity, activity, and long-term stability for the methanation of CO by compositional variation. A special challenge was the attempted selectivity improvement through doping and elemental variations, carried out by high-throughput technology (HTT). In the last decade, combinatorial and high-throughput techniques have been used successfully to speed up research and development in all fields of material science, including formulation of polymers, phosphors, and solid-state catalysts [14]. These methods enable the rapid synthesis and the analysis of many compounds with a high degree of automation and miniaturization. They provide an ideal tool to facilitate rapid discovery and optimization of new solid-state catalysts for the selective methanation of CO.

Here we report our results on the application of HTT based on emissivity-corrected infrared thermography (ecIRT) in a search for new catalyst compositions.

2. Strategy for the development of new CO methanation catalysts

The implementation of combinatorial and high-throughput techniques in the research and development of new complex materials has sparked a change from the conventional one-at-a-time experiments to a highly parallel approach in which numerous components are investigated simultaneously [14]. The application of automated synthesis and screening techniques allows preparation and screening of several hundred catalysts per day. But because the total number of multi-element combinations is nearly infinite, a suitable strategy must be found to enhance the probability of discovering superior candidates within a reasonable time frame and with a reasonable amount of experimental effort. We selected a combined knowledge-based and random-based approach to accelerate the discovery and optimization of new materials.

Fig. 1 depicts the general procedure for the development of better catalysts by HTT. The starting point of the study (pre-screening) comprised several libraries from previous projects containing more than 2000 binary, ternary, and quaternary metal oxides (mainly noble metal-free combinations of transition metals). Results from these screening experiments and

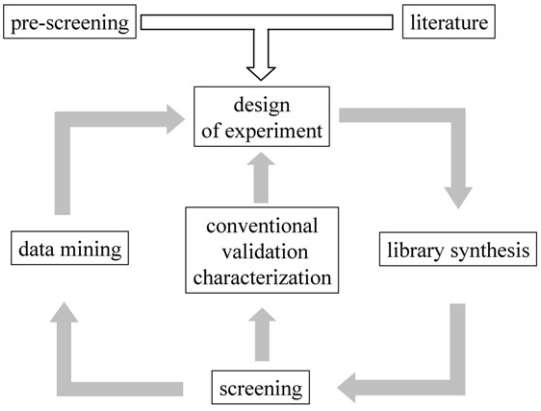

Fig. 1. The strategy for the combinatorial development of new catalysts.

literature data led to the selection of the most promising oxides, which presented the basis for synthesis of a still highly diverse set of starting libraries. Optimization and variation was realized in all generation libraries by composition spreads and by doping of initial hits with 50–60 different elements (usually in 2 concentrations). The automated synthesis of these libraries was performed with the help of a pipetting robot using sol–gel recipes and the library design software Plattenbau [15]. The sol–gel method allows the preparation of polynary mixed-metal oxides under mild synthesis conditions with a homogeneous elemental distribution and a high surface area. Furthermore, the use of identical preparation conditions for a highly diverse set of catalysts guarantees good comparability of the obtained data [16]. Parallel screening of the resulting libraries was performed by imaging the relative heats of reaction of >200 different catalysts using emissivity-corrected infrared thermography, followed by quantification of the individual heat spots with appropriate software. In general, the catalytic methanation of a typical hydrogen-rich reformate (containing ~1 vol% CO and considerable amounts of CO_2) at lower temperatures leads to preferential methanation of the monoxide (competitive hydrogenation), whereas at higher temperatures, the undesired hydrogenation of CO_2 increases [8–12]. In the isolated hydrogenation of CO_2 (solo methanation) the reaction rates are generally higher than those of isolated CO on various catalysts [17–19], indicating that CO competes successfully with CO_2 for active sites. Visualizing the relative heats of reactions, ecIRT provides no detailed information about the selectivity when different reactions occur simultaneously. Because the concentration of CO_2 is higher than that of CO in a reformate gas, CO_2 methanation can easily dominate the IR image under competitive reaction conditions. Therefore, we sequentially screened the activity of the different catalysts for the methanation of CO (1) and the methanation of CO_2 (2) at the same temperature:

$$CO + 3H_2 \leftrightarrows CH_4 + H_2O, \quad \Delta H^0_{500} = -214.4\ \text{kJ/mol} \qquad (1)$$

and

$$CO_2 + 4H_2 \leftrightarrows CH_4 + 2H_2O, \quad \Delta H^0_{500} = -174.6\ \text{kJ/mol}. \qquad (2)$$

The first measurements indicated that, compared with a typical reformate, a slightly higher concentration of CO in H_2 was

needed during the screening experiment to ensure good visualization of the respective reaction heat (signal intensity). Other components of a typical reformate, like N_2 and H_2O, were not considered in the high-throughput experiment (HTE). Conventional test experiments with reformate feed gas in the presence and absence of additional moisture revealed that the catalytic performance of the materials developed in the present study was not significantly affected by the presence of water in the reactant gas mixture, justifying our approach of disregarding it in the HTEs. The missing effect of water on the methanation performance was surprising but has been reported by others as well [11]. We hope to clarify this phenomenon in our ongoing studies. A typical gas sequence of a HTE at a given temperature was as follows:

- six-point temperature calibration in H_2;
- screening for CO methanation (2 vol% CO in H_2);
- flushing of the reactor with H_2;
- screening for CO_2 methanation (13 vol% CO_2 in H_2).

In each generation, the selection of new leads was based on the relative activity for the methanation of CO as well as the reactivity for the hydrogenation of CO_2. Due to the varying heats of reaction for (1) and (2) and the huge differences in the concentrations of the reactants, which were chosen similarly to the conventional gas mixture, the activity of a certain composition for the solo methanation of CO and of CO_2 could not be compared by the absolute increases in temperature during the corresponding reactions. Thus, we decided to rank the various catalysts of a given library according to their relative activity for the methanation of CO as well as that of CO_2 (1, best catalyst with highest heat of reaction; 206, worst material with the lowest heat of reaction). Consequently, each catalyst was characterized at a given temperature by a set of two numbers describing its relative activity for the solo methanation of CO and of CO_2 with respect to all other catalysts of the same high-throughput measurement. Comparisons of the respective rankings under the different gas mixtures were used as selectivity indicators. To identify materials with a high activity as well as selectivity for CO, leads are identified by high rankings for CO (1, 2, 3, ...) and moderate or low rankings for CO_2 (>30). In the advanced state of the optimization process, the long-term stability of the investigated samples was considered in addition to the CO activity and selectivity as further criteria for the selection of hits. Furthermore, all changes in the gas concentrations during HTEs were recorded by means of gas sensors to get information of the overall conversion under the various atmospheres of a certain library at a given temperature. Validation of the high-throughput results was achieved by scaling-up the most promising candidates of each generation and investigating them conventionally in a fixed-bed flow reactor. The testing conditions were chosen according to real requirements (high weight hourly space velocity, gas composition, and temperature). Selected samples also were tested in an industrial scale in the laboratories of Umicore AG & Co. KG. Characterization of the best conventional samples resting mainly on structural analysis provided more useful data that could be used together with all other information obtained within one developing stage to design the synthesis of the next catalyst generation. A MS-Access-based database developed in our group was used as a visualization and data mining tool [20].

3. Experimental

3.1. High-throughput syntheses of catalyst libraries

The synthesis of the catalyst libraries was performed automatically with the aid of a commercial pipetting robot (Lissy; Zinsser Analytic). The formation of the final reaction mixtures was achieved by transferring the required volumes of the different reagents in 10-ml vials into 2-ml vials arranged in racks of 50 vessels. Depending on the desired elemental composition of the catalyst, various metal precursors, solvents, and complexing agents had to be used according to the respective sol–gel recipe. Solutions of metal nitrates (Ag, Al, Ba, Ca, Ce, Co, Cr, Cu, Dy, Er, Eu, Fe, Ga, Gd, Ho, In, K, La, Li, Lu, Mg, Na, Nd, Ni, Pd, Pt, Pr, Sc, Sm, Sr, Tb, Tm, Y, Yb, and Zn), alkoxides (Al, Bi, Ge, Mn, Mo, Pd, Rb, Si, Ta, Ti, and V), halides (Au, Ba, Cs, Hf, Ir, Nb, Pt, Re, Rh, Ru, Sb, Sn, Sr, Te, and W) dinitrate oxide (Zr) and acid (B) were used as standard dopant solutions, whereas concentrations and solvents depended on the applied synthesis route. The concentration of the matrix metal stock solution was typically in the range of 1 M, and that of the dopants was in the range of 0.1–0.3 M.

The syntheses of all catalyst libraries were designed using the *Plattenbau* library design software [15]. Based on parameterized sol–gel recipes, this software calculated the volumes of the different reagents and created a pipetting list that could be transferred directly to the robot.

The preparation of the various catalyst libraries in this study rested on three different modified sol–gel recipes. The quantity of each catalyst synthesized in a HTE was defined by the total amount of metals, which typically was in the range of 300 μmol. Identification of the prepared samples is achieved by the nature and the concentration of the central elements. Because all catalysts were metal oxides with unknown oxidation states of the different metals, the samples are described by the metal ions and their mol% as a subscript; for instance, $Hf_9Ni_{91}O_x$ depicts an oxide of 9 mol% Hf and 91 mol% Ni.

3.1.1. Method 1. The propionate route [21]

This method allowed the preparation of Co-, Cr-, and Ni-based mixed oxides based on following molar ratio of metal(s):complexing agent (4-hydroxy-4-methyl-2-pentanone): alcohol (methanol, ethanol, and 2-propanol) of 1:3:50. The preparation of $Y_9Ni_{91}O_x$ for instance was carried out by pipetting following volumes of solutions in the described order: 567.7 μl of 2-propanol, 131 μl of 4-hydroxy-4-methyl-2-pentanone, 318.5 μl of Ni(II) propionate (1 M in methanol) and 90 μl of $Y(NO_3)_3 \cdot 6H_2O$ (0.35 M in methanol). After finishing all pipetting steps for the whole rack, the samples were placed in an orbital shaker (Titramax 100, Heidolph) for 1 h and dried for 5 days at room temperature and for an additional day at

40 °C. All samples were calcined under static air at 300 and 350 °C, respectively, for 5 h (heating rate, 60 °C/h).

3.1.2. Method 2. The ethylene glycol route [22,23]

Binary composition spreads $M_yM^*_{100-y}O_x$ with M and M* = Cr, Mn, Fe, Co, Ni, Cu, Ag, La, Ce and $y = 0$, 2, 10, 25, 50, 75, 90, 95, 98, 100 mol% as well as Mg-, Zn-, Ag-, Ce-, and Fe-based samples were prepared using this method. The molar ratio of metal(s):ethylene glycol:H_2O:$HNO_{3(conc)}$ was 1:18:37.5:4. For example, $Ce_{25}Ni_{75}O_x$ was synthesized by pipetting 347.2 µl of a 0.648 M $Ni(NO_3)_2{\cdot}6H_2O$ solution in a mixture of ethylene glycol and water [100/54], 115.7 µl of a 0.648 M $Ce(NO_3)_3{\cdot}6H_2O$ solution in a mixture of ethylene glycol and water [100/54], and 83.6 µl of nitric acid (65%). After finishing all pipetting steps of one rack, the samples were placed in an orbital shaker (Titramax 100, Heidolph) for 1 h. Subsequent thermal treatment, including drying and calcination, was performed under static air. All samples were heated at 80 °C for 12 h (heating rate: 20 °C/h) and at 105 °C for 60 h followed by 400 °C for 5 h (heating rate, 6 °C/h).

3.1.3. Method 3: The alkoxide route

V-, Al-, Zr-, and Si-based catalysts were synthesized by a modified sol–gel process described previously [24]. The preparation of Ti- and Mo-based samples followed a similar procedure to one reported previously [25], using 2-propanol, metal alkoxide precursor and dopand solutions, water, and catalytic amounts of hydrochloric acid. Depending on the hydrolysis rate of the applied alkoxide precursor, a complexing agent (4-hydroxy-4-methyl-2-pentanone) had to be added in several cases. For example, $Co_2Si_{98}O_x$ was prepared by pipetting 1024.1 µl of 2-propanol, 294 µl of 1 M $Si(OC_2H_5)_4$ solution in 2-propanol, 60 µl of 0.1 M $Co(NO_3)_3{\cdot}6H_2O$ solution in 2-propanol, and 124.4 µl of a 0.145 M HCl solution in a mixture of water and 2-propanol [7/100]. After finishing all pipetting steps of one rack, the samples were placed in an orbital shaker (Titramax 100, Heidolph) for 1 h, followed by drying for 5 days at room temperature before being calcined under static air at 300 °C for 5 h (heating rate, 60 °C/h).

All catalyst powders obtained using methods 1–3 were ground in flasks and transferred manually into 206 hexagonally positioned wells of a slate library plate.

3.2. High-throughput screening of catalyst libraries

The setup for the parallel investigation of the catalyst libraries by means of ecIRT, as well as its measurement principles, have been described in detail previously [26–28]. Briefly, the library was placed in a tightly closed gas-phase reactor with an IR-transparent sapphire window, allowing the in situ recording of temperature changes by an IR camera (PtSi 640, Thermosensorik). All processes, including gas dosing, temperature, and IR-camera control, were regulated automatically by our IR-Testrig software. Before all measurements, the catalyst libraries were pretreated reductively at 300 °C for 2 h in flowing H_2. Six-point temperature calibration was carried out in a range of −4 to +6 °C around the desired reaction temperature under the same gas atmosphere. CO methanation activity tests were performed in a mixture of 2 vol% CO in H_2 for 1 h. Before the CO_2 hydrogenation reactivity of the various samples with 13 vol% CO_2 in H_2 was investigated, the library was purged with H_2 for 30 min. The flow rate was 50 ml/min in all cases. The gas outlet of the reactor was connected to a set of IR gas sensors (customized production, GfG mbH) to acquire information about the integral conversion of a whole library. Long-term stability tests were performed by treating a certain library with a slightly modified reformate gas mixture ($CO/CO_2/N_2/H_2$ = 2/15/19/64; enriched with water) at 220 °C for approximately 100 h. Comparisons of the results of a habitual screening experiment (CO/H_2 followed by CO_2/H_2) performed before and after the long-term treatment were used to evaluate the long-term stability of the materials investigated.

3.3. Conventional catalyst syntheses

Ni-based catalysts were prepared conventionally following method 1 for a 20× larger scale (6 mmol). For example, $Ti_8Hf_9Ni_{83}O_x$ was synthesized by placing 5.35 ml of 2-propanol and 2.23 ml of 4-hydroxy-4-methyl-2-pentanone in a 20-ml vial. Subsequently, 4.98 ml of a 1 M Ni(II) propionate solution in methanol, 1.80 ml of a 0.3 M $HfCl_4$ solution in methanol, and 4.80 ml of a 0.1 M $Ti(OC_3H_7)_4$ solution in 2-propanol were added under stirring. The reaction mixture was stirred for 1 h and then dried for 5 days at room temperature, followed by 1–2 days at 40 °C. Calcination was carried out under static air at 300 and 350 °C, respectively, for 5 h at a heating rate of 60 °C/h. An industrial Ru/TiO_2 (4 wt%) supplied by Umicore AG & Co. KG was used as a reference material.

3.4. Conventional catalyst testing

Conventional catalytic tests were carried out in a tubular fixed-bed flow reactor at atmospheric pressure. To prevent methanation of CO_2 due to hot spot formation, 100 mg of the sample (100–200 µm) was diluted with 500 mg of quartz sand (100–200 µm). After a reductive pretreatment of all samples except the reference catalyst in flowing H_2 at 300 °C (flow rate, 100 ml/min) for 2 h, the reaction was started at a WHSV of 75,000 ml/(h g). In most cases, the reactant gas mixture ($CO/CO_2/N_2/H_2$ = 2/14.9/19.8/63.3) was enriched with water at room temperature by passing it through a washing bottle before the reactor. Experiments demonstrated good consistency between the theoretical amount for a water-saturated gas atmosphere and that found by differential weighing of water condensed in a cold trap for several hours under conditions comparable to the reaction. The total concentration of water was ca. 3 vol%. Analysis of the products was carried out using IR gas sensors (2 vol% CO, 25 vol% CO_2, and 20 vol% CH_4, GfG mbH).

Catalytic tests in the industrial laboratory were performed in a plate reactor under transient conditions at a heating rate

of 1 °C/min. Educt gas was fed between two plates coated with the catalyst powder. Similar to the experiments in academic laboratories, the catalysts were reduced in flowing H_2 at 300 °C before the reaction was started at a GHSV of 8000 h^{-1}. The more realistic reformate composition was $CO/CO_2/N_2/H_2O/H_2$ = 0.27/14.67/10/15.39/59.67. Analysis of the effluent gas was conducted online by NDIR (Emerson).

3.5. Catalyst characterization

Nitrogen physisorption measurements were performed on a Carlo Erba Sorptomatic 1990 at −196 °C. All samples were outgassed for 2 h under vacuum at 200 °C before adsorption. Powder X-ray diffraction (XRD) patterns were obtained using a Huber G670 Guinier image plate system with Cu$K_{\alpha 1}$-radiation ($\lambda = 1.54056$ Å). Crystal data as lattice constants, as well as mean particle sizes (d), were determined by Rietveld refinement using TOPAS software [29].

For temperature-programmed reduction (TPR), 45 mg of the catalyst was placed in the center of a gas-phase quartz reactor (3 mm i.d.) on quartz wool. The temperature of the catalyst was recorded by a thermocouple inside the catalyst bed, which was connected to a temperature controller (dTron 16.1; Jumo). The reactor tube was heated by an electric furnace (MTF 12/25/250; Carbolite). Before hydrogen consumption was measured, the catalyst was treated *in situ* at 200 °C in flowing N_2 (50 ml/min). After the sample was cooled to approximately 35 °C, the TPR was started in $H_2/N_2 = 10/90$ at a total flow rate of 50 ml/min and a heating rate of 5 K/min. The various gas compounds were analyzed online by quadrupole mass spectrometry (QMA 200, Pfeiffer vacuum). Hydrogen consumption was identified by normalizing the hydrogen intensity to the internal standard (nitrogen).

4. Results and discussion

4.1. High-throughput and conventional experiments of generations 1 and 2

Our strategy for the development of new catalytic materials was based on the evolutionary concept of variation and selection. Because activity as well as selectivity for the hydrogenation of CO are crucial in the purification of hydrogen-rich gas mixtures by means of the methanation reaction, selection of leads was based on the relative catalytic activity for the solo methanations of CO and of CO_2. Because both reactions are exothermic, the catalytic activity of a respective sample was correlated with the amount of heat generated during the solo hydrogenation. EcIRT was used to visualize the heats of reaction of all samples of a library under different atmospheres in a parallel approach. Rankings were applied to compare the relative activities of the various samples of a given library. Good rankings (1, 2, 3, …) during the solo methanation of CO combined with a moderate position (>30) during CO_2 methanation were considered to suggest good CO activity and selectivity. The hits of one generation were subsequently varied by compositional modification and doping in a search for improvement.

The active elements identified during the prescreening test with about 2000 samples on libraries available in the group (see above) and elements chosen from the literature led to the synthesis of the different starting libraries. Table 1 summarizes the sample composition, measurement temperatures, and hits of the various starting libraries, numbered sequentially.

Fig. 2 shows the emissivity-corrected IR-thermographic images of library 2 during the methanation of CO (a) and CO_2 (b) at 200 °C. Note that due to the higher concentration of the reactant in the CO_2/H_2 gas mixture, the absolute temperature increase during the methanation of the CO_2 was much higher than that during the methanation of CO in this generation. The

Table 1
Sample composition, reaction temperature and hits of the various diverse starting libraries

Library	Composition	Reaction temperature (°C)	Hits
1	$M_yM^*_{100-y}O_x$ with M and M* = Cr, Mn, Fe, Co, Ni, Cu, Ag, Ce, La and $y = 0$, 2, 10, 25, 50, 75, 90, 98, 100 mol%	160; 200; 230	$E_yNi_{100-y}O_x$ with E = Ce, Cr and $2 \leqslant y \leqslant 25$ mol%; $E_yCe_{100-y}O_x$ with E = Ni, Cr and $0 \leqslant y \leqslant 25$ mol%
2	$M_yM^*_{100-y}O_x$ with M and M* = Cr, Mn, Fe, Co, Ni, Cu, Ag, Ce, La and $y = 0$, 2, 10, 25, 50, 75, 90, 98, 100 mol% $E_yNi_{100-y}O_x$ with $y = 2$ and 10 mol%	160; 200; 230	$E_yNi_{100-y}O_x$ with E = Y, Ce, Hf, Cr, rare earth metals and $y = 2$ and 10 mol%
3	$E_yMo_{100-y}O_x$, $E_yAg_{100-y}O_x$ with $y = 2$ and 10 mol%	200; 250; 300	–
4	$E_yCo_{100-y}O_x$, $E_yCe_{100-y}O_x$ with $y = 2$ and 10 mol%	160; 180; 200; 230	$E_yCe_{100-y}O_x$ with E = V, B, Cs (Rb, Ge, Zr, Mo) and $y = 2$ and 10 mol%
5	$E_yCe_{100-y}O_x$, $E_yFe_{100-y}O_x$ with $y = 2$ and 10 mol%	180; 200; 230; 250; 300	$E_yFe_{100-y}O_x$ with E = Li, Na, K, Rb and $y = 2$ and 10 mol%
6	$M_yM^*_{100-y}O_x$ with M = Ag, Ce, Co, Fe, Ir, Ni, Pd, Pt, Re, Rh, Ru and M* = Al, Cr, Mg, Si, Ti, V, Zn, Zr with $y = 2$ and 6 mol%	200; 250; 300	$M_yMg_{100-y}O_x$, $Rh_yV_{100-y}O_x$ and $Co_yV_{100-y}O_x$

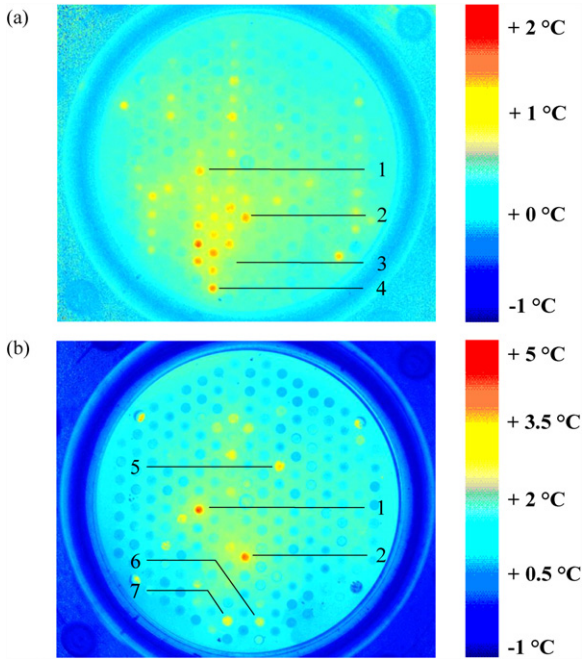

Fig. 2. Emissivity-corrected IR-thermographic images of catalyst library 2 during methanation of CO (a) and of CO_2 (b) at 200 °C. 1: $Ce_{10}Ni_{90}O_x$; 2: $Cr_{10}Ni_{90}O_x$; 3: $Ni_{100}O_x$; 4: $Sm_{10}Ni_{90}O_x$; 5: $Cu_{10}Ag_{90}O_x$; 6: $Cu_2Ag_{98}O_x$; 7: $Ag_{100}O_x$.

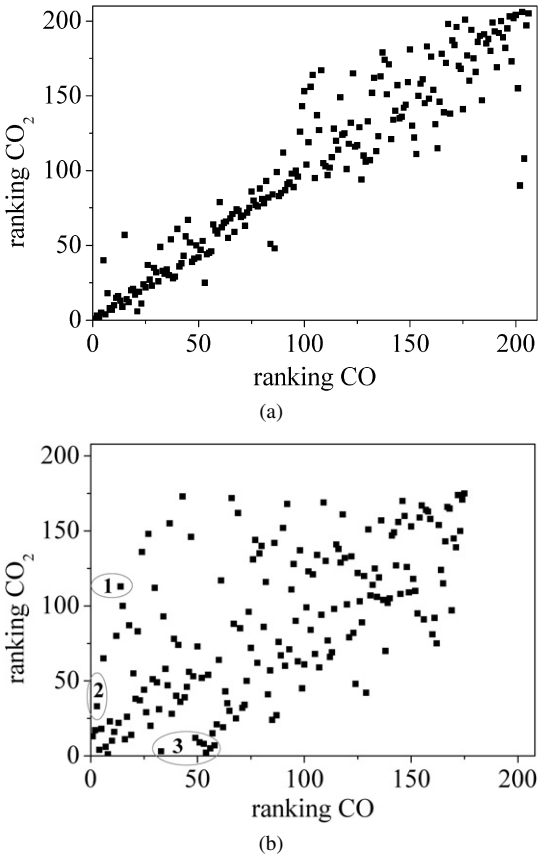

Fig. 3. Comparison of the catalysts' rankings on library 4 (a) and on library 2 (b) in hydrogenation of CO and CO_2 after 60 min at 200 °C. 1: $Hf_2Ni_{98}O_x$; 2: $Y_2Ni_{98}O_x$; 3: Co-, Cr-, Fe-, and Cu-doped Ag.

Ni-based catalysts performed the best of all the samples tested. The addition of the doping elements Cr, Y, and several rare earth metals, such as Ce, Ho, Nd, or Sm, led to a dramatic increase in the solo methanation activity of CO compared with the undoped Ni, which demonstrated no activity under the reaction conditions used here.

Under CO_2/H_2 atmosphere, several compositions of the same library revealed quite astonishing behavior. It is well known that typical methanation catalysts based on Ru or Ni generally provide higher reaction rates in the solo methanation of CO_2 relative to that of CO [17–19]. Thus, a linear correlation between the relative rankings of the various catalysts under CO/H_2 and CO_2/H_2 could be expected, as found in, for instance, the methanation reactions of doped Ce- and Co-based mixed oxides on library 4 (Fig. 3a). In such a plot, the desired materials are found in the upper left corner with a high ranking (small number) for CO methanation and a low ranking (large number) for CO_2 methanation. Such a behavior was found in the case of library 2 (Fig. 3b) with such compositions as $Ce_{10}Ni_{90}O_x$ or $Cr_{10}Ni_{90}O_x$, featuring high relative activities for the solo methanation of both CO and CO_2, whereas the addition of Hf seemed to decrease the net reactivity with respect to CO_2, in contrast to CO (catalyst 1 in Fig. 3b). Although Ag-based catalysts were marginally active in the hydrogenation of CO in the investigated temperature range, they revealed relatively high heats of reaction during the methanation of CO_2. As shown in Table 1, various hits could be found on other starting libraries under the given reaction conditions. Traditional CO hydrogenation metals, such as Fe or even Ce, exhibited upon doping activity for the investigated reaction. Considering the reaction temperatures as well as the particular overall conversions of all examined libraries monitored by IR gas sensors during all reactions, only Ni- and partly Ce-based samples were taken into account as base materials for the subsequent generations. Overall, Y-, Hf-, Ho-, Cr-, Ce-, and Sm-doped Ni catalysts were selected as hits from the respective libraries. The results of our screening experiments with the starting libraries are in agreement with data reported in the literature. The increased CO methanation rate resulting from reduced Co and Ni was reported at the beginning of the last century by Sabatier and Senderens [30]. Recently, other authors [17] investigated the influence of Sm_2O_3 on the catalytic activity and long-term stability of a ZrO_2-supported Ni methanation catalyst. Several papers deal with the promoting effect of TiO_2 [31] and of rare earth metals on a Ni/γ-Al_2O_3 catalyst [32,33] resting mainly on enhancement of the active site dispersion as well as electronic effects. To the best of our knowledge, improved performance of a Ni-based methanation catalyst by Hf has not yet been described in the literature. All selected leads were conventionally prepared and tested to evaluate the results of the HTEs under CO/CO_2 competition with the more realistic reformate gas mixture (not shown).

In the second catalyst generation, the effect of the doping element contents was studied by means of compositional variation within the range of 0–50 mol%. The so-identified hits were subsequently upscaled and tested in the fixed-bed flow reactor. Fig. 4a compares the results of the conventional experiments

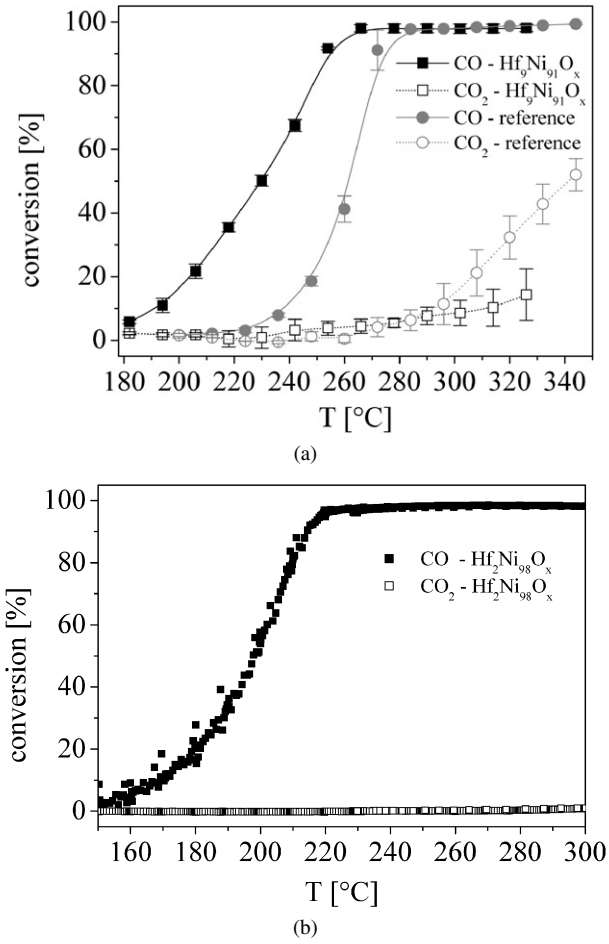

Fig. 4. (a) Comparison of the conventional results of $Hf_9Ni_{91}O_x$ with an industrial reference. Operating conditions: $P = 1$ bar; total flow rate: 125 ml/min ($CO/CO_2/N_2/H_2 = 2/14.9/19.8/63.3$; enriched with water at room temperature); catalyst weight: 100 mg diluted with 500 mg quartz sand (both 100–200 μm). CO conversion (■) and CO_2 conversion (□) of $Hf_9Ni_{91}O_x$; CO conversion (●) and CO_2 conversion (○) of the reference catalyst. (b) Influence of the reaction temperature on the conversions of CO and CO_2 over $Hf_2Ni_{98}O_x$ under industrial testing conditions: $P = 1$ bar, GHSV = 8000 h^{-1} ($CO/CO_2/N_2/H_2O/H_2 = 0.27/14.67/10/15.39/59.67$).

of $Hf_9Ni_{91}O_x$ with those of the industrial reference catalyst Ru/TiO_2 (4 wt%). It should be mentioned that in contrast to the traditional procedure of applying a reductive pretreatment to all catalysts, the reference had to be investigated with no prereduction. On supported Ru, CO is hydrogenated preferentially, whereas the reaction of CO_2 occurs at higher temperatures after most of the CO is converted. This behavior during the competitive methanation of CO and CO_2 is well known and can be ascribed to stronger interactions of the CO molecule with the catalytically active sites compared with CO_2 [8,9,11]. Apparently, CO_2 conversion can occur only when most of the CO is converted, freeing active sites. Typical Ru- or Ni-based catalysts behave similarly to the reference by providing preferable conversion of CO over a temperature range of approximately 20–40 °C, whereas undesired methanation of CO_2 dominates at higher temperatures [8–11]. Compared with the reference, $Hf_9Ni_{91}O_x$ exhibited higher catalytic activity for the hydrogenation of CO, whereas reactivity for the methanation of CO_2 was drastically decreased at the same time. Respective investigations with the first-generation catalyst $Hf_2Ni_{98}O_x$ in the laboratories of Umicore AG & Co. KG confirmed this surprising activity- and selectivity-increasing effect of Hf doping on Ni oxide. As shown in Fig. 4b, almost full conversion of CO could be achieved at 230 °C, whereas practically no CO_2 reacted over the entire temperature range examined. The good comparability of the data obtained in the various laboratories also demonstrates that the catalytic performance of the samples investigated here is not sensitive or only marginally sensitive to the water content of the gas mixture used.

In general, the key properties of the examined materials cannot be easily identified by such established factors as conversion or selectivity. Selectivity is especially difficult to assess, because the CO_2 concentration is much higher than the CO concentration, and CO_2 hydrogenation is strongly dependent on CO concentration. Therefore, we have developed another set of identifiers, three temperatures that describe the properties of the investigated catalysts:

- T_{50} (°C): Temperature at which 50% of CO is converted. Due to the higher concentration of CO (2 vol%) in the reaction gas mixture used in this study compared with realistic feeds (0.3–1 vol%); this temperature was chosen as benchmark for the lowest possible working temperature of the various catalysts. Respective tests in industrial laboratories under realistic conditions (larger scale of the setup, lower CO concentration, and higher H_2O content) were in good agreement with this assumption.
- T^*_{10} (°C): Temperature at which 10% of CO_2 is converted. Because of the exothermic character of both hydrogenation reactions, hot spot formation associated with the methanation of CO_2 could dramatically increase the undesired consumption of H_2. Thus, a catalyst that effectively hydrogenates CO over a wide temperature region in which the conversion of CO_2 is only marginally affected by the temperature is preferable. The difference between T_{50} and T^*_{10} was used to identify the temperature range of highly selective CO conversion.
- T^*_{20} (°C): Temperature at which 20% of CO_2 is converted. The reactivity for the methanation of CO_2 at temperatures higher than the preferred working temperature range is described by the difference between T^*_{20} and T^*_{10}.

In principle, T_{50} should be as low as possible, because the desired process temperature should be in the range of the low-temperature water–gas shift reaction, which generally occurs at around 200 °C [1]. Moreover, the influence of the water–gas shift equilibrium, which favors the formation of CO by partial hydrogenation of CO_2 at elevated temperatures, is reduced at low temperatures. Most importantly, the temperature difference $T^*_{10} - T_{50}$ should be as large as possible to separate the two competing reactions. The temperature difference $T^*_{20} - T^*_{10}$ also should be as large as possible and can be interpreted as an indicator of the CO_2 conversion rate. If it is small, as with most literature catalysts or the reference catalyst, then CO_2 conversion increases, resulting in undesired H_2 consumption. The

Table 2
Comparison of the conventional results of various generation 2 catalysts with an industrial reference as well as the undoped generation 0 catalyst. Operating conditions: $P = 1$ bar; total flow rate: 125 ml/min ($CO/CO_2/N_2/H_2$ = 2/14.9/19.8/63.3; enriched with water at room temperature); catalyst weight: 100 mg diluted with 500 mg quartz sand (both 100–200 μm)

Catalyst	T_{50} (°C)[a]	T^*_{10} (°C)[b]	T^*_{20} (°C)[c]
Reference	262	294	307
$Ni_{100}O_x$	308	334	359
$Hf_9Ni_{91}O_x$	232	312	341
$Y_9Ni_{91}O_x$	224	248	260
$Ho_{18}Ni_{82}O_x$	233	261	272
$Cr_6Ni_{94}O_x$	210	240	252
$Sm_{12}Ni_{88}O_x$	232	252	267
$Ce_{15}Ni_{85}O_x$	220	249	261
$Ce_{25}Ni_{75}O_x$	215	242	262

[a] Temperature where 50% CO were converted.
[b] Temperature where 10% CO_2 were converted.
[c] Temperature where 20% CO_2 were converted.

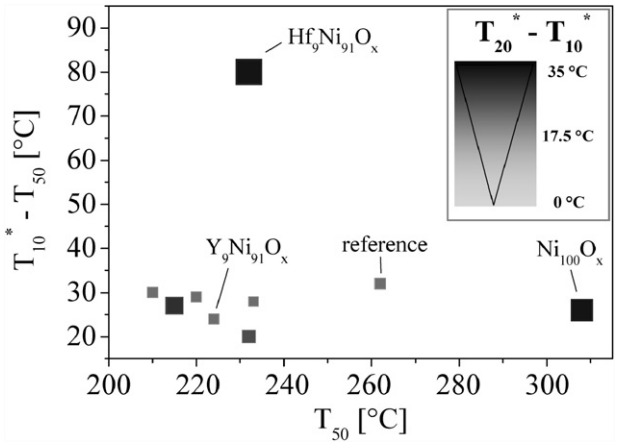

Fig. 5. Results of the conventional experiments of generation 2 catalysts compared to the reference catalyst and the undoped base metal. Operating conditions: $P = 1$ bar; total flow rate: 125 ml/min ($CO/CO_2/N_2/H_2$ = 2/14.9/19.8/63.3; enriched with water at room temperature); catalyst weight: 100 mg diluted with 500 mg quartz sand (both 100–200 μm).

composition and the results of the various samples investigated conventionally in the second generation are summarized in Table 2. All findings were compared with the reference catalyst as well as with the undoped Ni catalyst. Fig. 5 visualizes these achievements by plotting T_{50} versus the width of the appropriate working temperature range ($T^*_{10} - T_{50}$). The temperature difference $T^*_{20} - T^*_{10}$ is illustrated by the size and the color of the respective data points. Compared with the industrial reference material, all samples prepared within this study behave differently. For instance, the catalytic activity of the undoped Ni catalyst was much too low for a potential industrial application, because performing the methanation reaction in the range of 200–250 °C is favorable. In addition, high conversion of CO could not be achieved on undoped Ni due to an overlap of hydrogenation of both CO and CO_2 and/or a reverse water–gas shift reaction (see Fig. 9 below). All second-generation catalysts, on the other hand, are more active than the reference. These samples can be classified in two different groups (see Fig. 5). The first group, consisting of $Y_9Ni_{91}O_x$, $Ho_{18}Ni_{82}O_x$, $Cr_6Ni_{94}O_x$, $Sm_{12}Ni_{88}O_x$, $Ce_{15}Ni_{85}O_x$, and $Ce_{25}Ni_{75}O_x$, converted 50% CO at temperatures as low as 210–235 °C, with Ce and Cr doping resulting in the highest activities. Sm- and Ho-doped Ni catalysts, on the other hand, were least active within this class of samples. The reference catalyst, in contrast, required a temperature above 260 °C. The second group consisted of just the already described $Hf_9Ni_{91}O_x$, which demonstrated a significant catalytic performance by guaranteeing high conversion of CO at relatively low temperatures with negligible methanation of CO_2 over a range of ca. 80 °C. To the best of our knowledge, this high catalytic activity in the hydrogenation of CO combined with such low reactivity for the conversion of CO_2 is unique for this application. These results are in full agreement with the respective HTEs. Comparing the relative rankings in the methanation of CO with those during the conversion of CO_2, especially Hf-doped Ni oxides, provided relatively high rankings for the conversion of CO combined with low rankings for that of CO_2, whereas doping with Cr, Ce, Sm, Ho, and Y resulted primarily in high rankings for CO (Fig. 3b). The conventional validations impressively displayed the potential of our approach in investigating the reactivity of a catalyst library in converting various compounds of a gas mixture separately to screen for activity as well as selectivity in a parallel manner. All in all, $Y_9Ni_{91}O_x$ as atypical methanation catalyst, as well as $Hf_9Ni_{91}O_x$ converting CO extremely selectively over a wide temperature range, have been selected as hit samples of the second-generation catalysts.

4.2. High-throughput and conventional experiments of generation 3

The effect of a third metal on the catalytic performance of the leads was investigated by doping $Hf_9Ni_{91}O_x$ and $Y_9Ni_{91}O_x$ [library 8] with nearly 60 elements usually in two different concentrations, except for the noble metals, which were applied only in the smaller concentration. The selection of hits was based on CO activity and selectivity, as well as on long-term stability. For long-term stability, the whole library was exposed to a more realistic gas mixture ($CO/CO_2/N_2/H_2$ = 2/15/19/64, enriched with water) at 220 °C for ca. 100 h. Standard screening experiments (investigations in CO/H_2 followed by CO_2/H_2) were performed before and after the long-term treatment, whereas the results of the latter ones were considered for selection based on both activity and selectivity. Monitoring of the total gas composition during the complete experiment by means of gas sensors demonstrated no decline in the catalytic activity of the whole library, giving rise to the assumption that the Ni-based catalysts investigated here exhibited good long-term performance. Comparison of the overall conversions during the solo methanation of CO_2 of the respective first-generation library with that of the third-generation library demonstrated a dramatic decrease in CO_2 reactivity within our developing process at comparable activities for the methanation of CO, indicating that the doping elements strongly affect the selective nature of the active sites. For instance, the overall CO_2 conversions of library 2 during solo methanation of the corre-

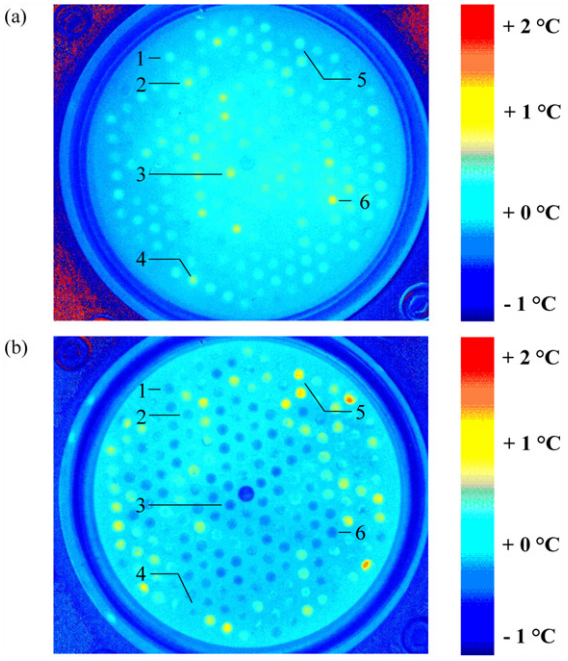

Fig. 6. Emissivity-corrected IR-thermographic images of catalyst library 8 during methanation of CO (a) and of CO_2 (b) at 200 °C. 1: $Ti_8Hf_9Ni_{83}O_x$; 2: $Ru_2Y_9Ni_{89}O_x$; 3: $Rh_2Hf_9Ni_{89}O_x$; 4: $Re_2Y_9Ni_{89}O_x$; 5: $Tm_2Hf_9Ni_{89}O_x$; 6: $Ir_2Hf_9Ni_{89}O_x$.

sponding carbon oxide varied between 70 and 80% at 200 and 230 °C, whereas library 8 converted only approximately 10% under the same reaction conditions. This significant increase in selectivity, which rested on the applied strategy of hit selection was also reflected in the analogous IR-thermographic images. Due to the huge content of CO_2 compared to CO, the temperature increase during the solo methanation of CO_2 on library 2 was (due to the high conversions) much higher than that during the conversion of CO (Fig. 2). On the other hand, the absolute temperature increases in the third-generation library were comparable under both gas mixtures, as shown in Fig. 6, which displays the emissivity-corrected IR-thermographic images of library 8 during the methanation of CO (a) and CO_2 (b) at 200 °C. Furthermore, a group of catalysts showed high activity for the hydrogenation of CO but no increase in temperature during the reaction of CO_2 as for, for instance, $Re_2Y_9Ni_{89}O_x$ or $Ir_2Hf_9Ni_{89}O_x$ on library 8 (Fig. 6, samples 4 and 6). Comparisons of the relative rankings under the various gas mixtures were used to visualize this phenomenon. As depicted in Fig. 7, the addition of Re, Ru, Rh, Ir, and partly Pd and Au as third metals to the different binary Ni-based catalysts resulted in a conspicuous decrease in the relative reactivity for the methanation of CO_2, whereas the high rankings for CO argue for good CO methanation activity. This discovery was very surprising, because first, the doping of the pure Ni in the first-generation catalyst with these metals improved neither the catalytic activity nor the selectivity of the materials, and second, most of these elements are well known for their methanation activity and thus were expected to act as activity-improving rather than selectivity-improving components. Furthermore, $Ti_8Hf_9Ni_{83}O_x$ as noble metal free sample in this

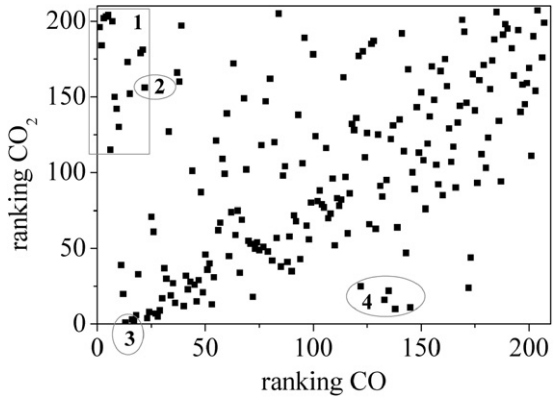

Fig. 7. Comparison of the catalysts' rankings on library 8 in hydrogenation of CO and CO_2 after 60 min at 200 °C. 1: $D_2E_9Ni_{89}O_x$ with D = Re, Ir, Pt, Ru, Rh, (Pd, Au); E = Y and Hf; 2: $Ti_8Hf_9Ni_{83}O_x$; 3: $Tm_2Hf_9Ni_{89}O_x$, $Ho_8Y_9Ni_{83}O_x$, and $Gd_2Y_9Ni_{89}O_x$; 4: $D_8Y_9Ni_{83}$ with D = Tb, Gd, Nd, Ca, and Sr.

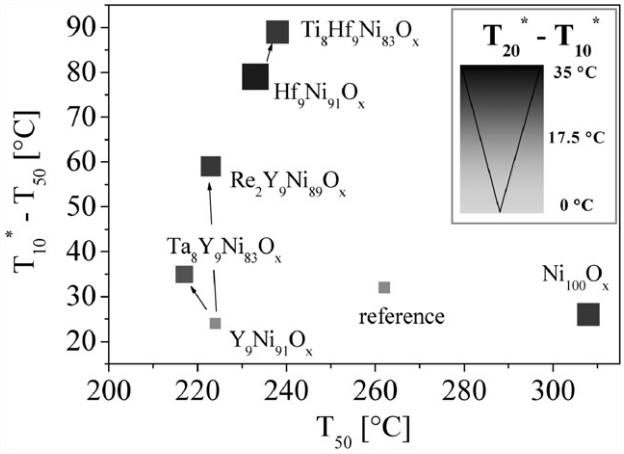

Fig. 8. Results of the conventional experiments of generation 3 catalysts compared to the reference catalyst and the undoped base metal. Operating conditions: $P = 1$ bar; total flow rate: 125 ml/min ($CO/CO_2/N_2/H_2$ = 2/14.9/19.8/63.3; enriched with water at room temperature); catalyst weight: 100 mg diluted with 500 mg quartz sand (both 100–200 μm).

formerly discussed group of catalysts demonstrated similar catalytic performance in the various gas mixtures compared with the noble metal-containing samples, suggesting the very high CO selectivity of this material (Fig. 6, sample 1; Fig. 7, sample 2). The addition of other doping elements to the Ni-based systems (e.g., Tm, Ho, Nd, or Gd) seemed to improve the activity for the unwanted methanation of CO_2 (Fig. 6, sample 5; Fig. 7, samples 3 and 4).

Fig. 8 summarizes the results of the conventional validation of selected third-generation catalysts. In agreement with the drastic decline in the total CO_2 hydrogenation reactivity observed during HTE with the respective catalyst library, all conventionally investigated samples are characterized by a distinct increase in CO selectivity. The addition of 2 mol% Re, for instance, expanded the appropriate working temperature range of $Y_9Ni_{91}O_x$ from approximately 25 °C to almost 60 °C, whereas the CO activity described by T_{50} was comparable for both samples. This decreased CO_2 reactivity was also reflected in a considerable increase in $T_{20}^* - T_{10}^*$ for the Re-modified ma-

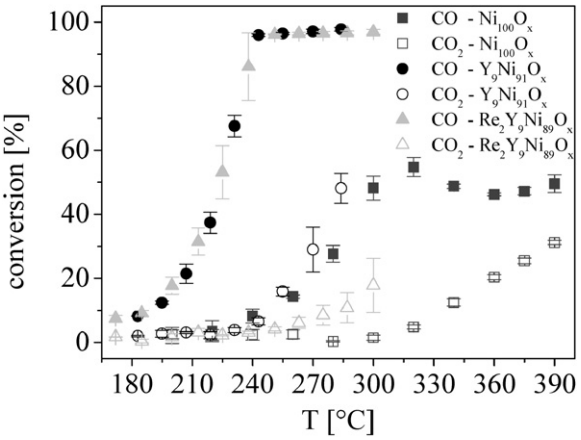

Fig. 9. Optimization of Ni-based catalysts with respect to CO activity and selectivity. Operating conditions: $P = 1$ bar; total flow rate: 125 ml/min ($CO/CO_2/N_2/H_2 = 2/14.9/19.8/63.3$; enriched with water at room temperature); catalyst weight: 100 mg diluted with 500 mg quartz sand (both 100–200 μm). CO conversion (■) and CO_2 conversion (□) of $Ni_{100}O_x$; CO conversion (●) and CO_2 conversion (○) of $Y_9Ni_{91}O_x$; CO conversion (▲) and CO_2 conversion (△) of $Re_2Y_9Ni_{89}O_x$.

terial. Fig. 9 clarifies the improved catalytic performance during the optimization process on the basis of the Y–Ni system. Starting with the neither active nor selective Ni oxide, doping with 9 mol% of Y produced a significantly enhanced catalytic behavior. Under competitive methanation conditions, the resulting $Y_9Ni_{91}O_x$ acted comparably to typical methanation catalysts by converting CO preferentially at lower temperatures and also CO_2 at elevated temperatures at which CO conversion was complete. Further doping of $Y_9Ni_{91}O_x$ with Re led to a definite change in the reactivity of the catalyst. Whereas the CO hydrogenation activity of $Y_9Ni_{91}O_x$ was affected only marginally by the third metal, $Re_2Y_9Ni_{89}O_x$ produced a greatly decreased reactivity toward CO_2 methanation. A principally analogous modification was observed by doping $Y_9Ni_{91}O_x$ with 8 mol% of Ta even, though the increase in selectivity was clearly smaller than in the case of $Re_2Y_9Ni_{89}O_x$ (Fig. 8). A similar effect arose from the addition of 8 mol% of Ti to the already highly selective $Hf_9Ni_{91}O_x$, the working temperature range of which increased to 90 °C.

Fig. 10 emphasizes this unique performance of the catalysts developed in this study by comparing the temperature dependence of the conversions of CO and of CO_2 on $Re_2Y_9Ni_{89}O_x$ (a) and on $Ti_8Hf_9Ni_{83}O_x$ (b) with those of the industrial reference. Providing higher activity in the hydrogenation of CO, the conversion of CO started at much lower temperatures on both Ni-based catalysts compared with the reference, whereas the absolutely undesired conversion of CO_2 was never much higher on both $Re_2Y_9Ni_{89}O_x$ and $Ti_8Hf_9Ni_{83}O_x$ over the temperature range investigated. The superior catalytic performance of the Ni-based samples is demonstrated by the wide working temperature range of $Re_2Y_9Ni_{89}O_x$ and $Ti_8Hf_9Ni_{83}O_x$, compared to the narrow temperature range of the reference, denoted by the corresponding bars on top of Fig. 10. The dramatic reduction in CO_2 reactivity, especially in the case of $Ti_8Hf_9Ni_{83}O_x$, is also reflected in the very smooth slope of the respective temperature-dependent function of the CO_2 conversion compared with the

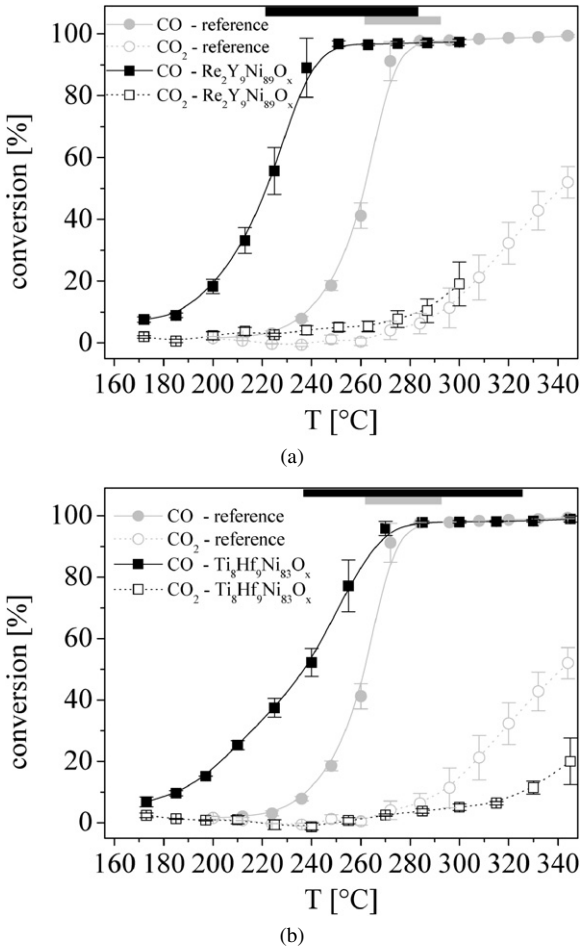

Fig. 10. Comparison of the conventional results of $Re_2Y_9Ni_{89}O_x$ (a) and of $Ti_8Hf_9Ni_{83}O_x$ (b) with an industrial reference. Operating conditions: $P = 1$ bar; total flow rate: 125 ml/min ($CO/CO_2/N_2/H_2 = 2/14.9/19.8/63.3$; enriched with water at room temperature); catalyst weight: 100 mg diluted with 500 mg quartz sand (both 100–200 μm). CO conversion (■) and CO_2 conversion (□) of $Re_2Y_9Ni_{89}O_x$ (a) and of $Ti_8Hf_9Ni_{83}O_x$ (b); CO conversion (●) and CO_2 conversion (○) of the reference catalyst. Bars on top indicate the respective working temperature range.

reference, indicating only a slight influence of the reaction temperature on the methanation of CO_2. Thus, our samples exhibit ideal catalytic behavior for the removal of CO from hydrogen-rich gas mixtures by means of methanation reaction, providing high catalytic activity for the conversion of CO combined with very low CO_2 methanation reactivity. The latter is important, because it may eliminate the problem of considerable hydrogen loss due to hot spot-induced autocatalytic methanation of CO_2. Due to the technology applied here, which includes reductive conditioning as well as long-term treatments of complete catalyst libraries, our materials would be expected to have good long-term stability. Verification experiments are currently underway.

4.3. Catalyst characterization

This study has demonstrated that even for relatively complex requirements, such as selective hydrogenation, tailor-made catalysts can be developed by directed elemental variation. The

Table 3
Overview on physical properties of selected catalysts. Lattice constants as well as medium particle sizes are related to the crystalline NiO (JCPDS: 73-1519). Given in parentheses is the standard deviation for the last indicated number

	S_{BET} (m^2/g)	Maximum pore radius (nm)[a]	a (Å)	d (nm)
$Ni_{100}O_x$	43	6.75	4.179(1)	17.1(1)
$Y_9Ni_{91}O_x$	96	3.65	4.1737(2)	10.7(1)
$Re_2Y_9Ni_{89}O_x$	130	1.83	4.183(1)[b]	32(3)[b]
$Hf_9Ni_{91}O_x$	29	1.77	4.184(1)[b]	42(15)[b]
$Ti_8Hf_9Ni_{83}O_x$	88	1.87	4.188(2)	9.9(2)[b]

[a] Determined from desorption branch following the BJH method.
[b] Poor crystallinity.

various dopants that were found to improve the catalytic properties of the matrix element Ni during the optimization process can be roughly classified into (i) activity-increasing elements causing greater CO and CO_2 methanation reactivity (e.g., Ce, Cr, Ho, Sm, Y) and (ii) selectivity-enhancing modifiers, the addition of which results mainly in decreased reactivity toward CO_2 while affecting CO activity only marginally (e.g., Pt, Re). Furthermore, the chemical element Hf seems to unify the features of both groups.

Standard characterization techniques have been applied to analyze the effect of diverse doping elements on structural properties of the investigated Ni-based oxides. Table 3 summarizes the effect of these elements on the BET surface area, pore structure, and crystalline parts of selected methanation catalysts. It is apparent that the addition of 9 mol% of Y to the pure $Ni_{100}O_x$ leads to a distinct change in the porous structure, resulting in increased specific surface area and a modified pore size distribution. Similar effects were found for other dopants assigned to the activity-increasing elements in the second generation as Cr or Ce (not shown). The modification of $Ni_{100}O_x$ with Hf also led to an evident change in the porous structure, with a significant decrease in the surface area of $Hf_9Ni_{91}O_x$ compared with that in undoped $Ni_{100}O_x$. Further addition of 8 mol% Ti resulted in a further increase in the surface area. The type of crystalline phase that could be detected by XRD was not affected by the modifications: cubic NiO (JCPDS 73-1519) was dominant in all of the diverse catalysts. Except for $Re_2Y_9Ni_{89}O_x$, which exhibited some very poor reflexes corresponding to the metallic Ni (JCPDS 87-0712), no other phases could be identified in the various metal oxides. Rietveld refinement was performed to obtain more detailed information on these crystalline parts. As shown in Table 3, the lattice constant a of cubic $Ni_{100}O_x$ was affected by the various dopants, whereas no clear trends were apparent. The addition of 9 mol% of Y resulted in, for instance, a decrease in the lattice constant from 4.179(1) Å to 4.1737(2) Å, whereas further modification with 2 mol% of Re led to an increase to 4.183(1) Å, giving rise to the assumption that some of the Ni sites in the crystalline structures might be replaced by other cations. Accordingly, due to higher charges of the replacing cations (e.g., Y^{3+}, Hf^{4+}, Re^{6+}) additional vacancies must be generated to maintain a charge balance, changing the sign of the lattice parameter even in the case of cations of smaller ionic radius, such as Ni^{2+} (CN = 6), to an open-ended question, not excluding oxygen vacancies (compare, e.g., the

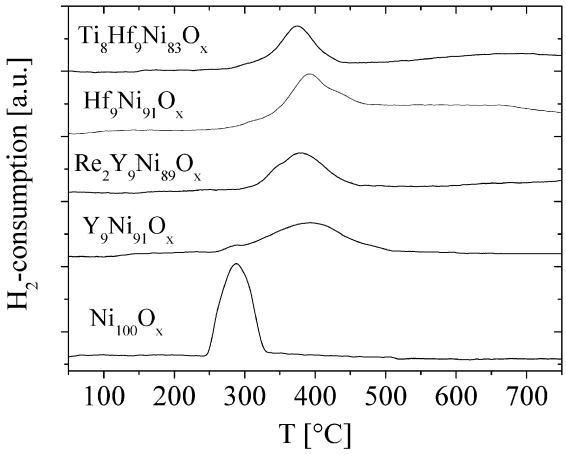

Fig. 11. TPR profiles of diverse Ni-based oxides.

crystal structures of NiO and ReO_3). The crystallinity as well as the mean particle size on the other side were greatly affected by the element(s) added.

TPR experiments were carried out to investigate potential interactions between the different components of the polynary oxides. Fig. 11 compares the TPR curve of the undoped $Ni_{100}O_x$ with the respective signals of the binary or ternary oxides. The pure Ni oxide showed a sharp hydrogen-consumption peak between 245 and 335 °C with a peak maximum temperature (T_{max}) of approximately 288 °C, corresponding to the reduction of the Ni oxide to the metallic Ni. The modification of this oxide with Y resulted in a definite change in the chemical reactivity. Only a few Ni species exhibited reductivity comparable to that of the undoped oxide; most were much more stable in the modified sample, as demonstrated by the main hydrogen consumption peak ranging from ca. 300 to more than 500 °C ($T_{max} = 393$ °C). This drastic change in the chemical properties on doping clearly demonstrates the high degree of interaction between the various components of this oxide. These interactions likely are related to bridging oxygen atoms between the various metals, with Y^{3+}-ions stabilizing the doped oxide compared with the pure $Ni_{100}O_x$. The wide temperature range of hydrogen consumption in $Y_9Ni_{91}O_x$ suggests the various interactions that could originate in various Ni–O–Y-constellations in the three-dimensional network. XRD analysis of samples after the TPR experiments identified a metallic Ni phase (JCPDS 87-0712) along with the oxide Y_2O_3 (JCPDS 43-1036), suggesting that hydrogen consumption relied only on the reduction of oxidic Ni species (i.e., spatial areas of the dopant distribution function with high Ni content). The further addition of Re resulted in a similar TPR profile for $Re_2Y_9Ni_{89}O_x$. Although the bimodal hydrogen consumption was still evident, no unmodified Ni species (which behave comparably to $Ni_{100}O_x$) could be found. Furthermore, the consumption signal was narrower than that of the binary $Y_9Ni_{91}O_x$. These findings indicate that Re plays an important role in the three-dimensional network as some kind of "mediator" among the various components of the Ni–O–Y-system by making them chemically more equal compared with $Y_9Ni_{91}O_x$.

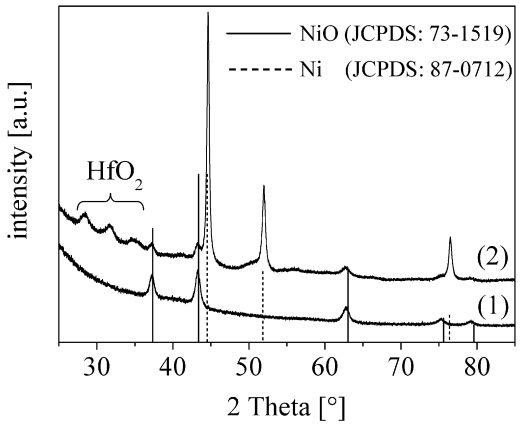

Fig. 12. Comparison of the XRD patterns of $Hf_9Ni_{91}O_x$ in the as-prepared state (1) with that of $Hf_9Ni_{91}O_x$ after reaction (2).

Compared with Ni^{2+} (crystal radius $cr^{[6]} = 0.83$ Å for CN = 6), the radii of Y^{3+} ($cr^{[6]} = 1.04$ Å) and Re^{6+} ($cr^{[6]} = 0.69$ Å) [34] deviate in different directions. Thus, in co-doping of both Y^{3+} and Re^{6+}, local distortions in coordination induced by one ion are damped by the presence of the other. The dramatic increase in the BET surface area, along with the change in the porous structure of this binary oxide on modification with Re (see Table 3), are indicative of a dramatic change in the microstructure. No definite Re structures could be identified by XRD. The absence of a (new) reduction peak in the respective TPR curve (as was expected at comparatively low temperatures for pure ReO_x species), combined with the changes in reactivity of the oxide and the porous structure discussed previously point to a (at least relatively) high homogeneous distribution of the various elements. Comparable results could be achieved by analyzing the reduction behavior of the Hf-modified samples. The cations of the relatively stable TiO_2 and HfO_2 increased the stability of the oxidic Ni species compared with the undoped $Ni_{100}O_x$. In analogy to the Y-modified system, the metallic Ni phase (JCPDS 87-0712) and a HfO_2 phase (JCPDS 74-1506) were detected after the TPR experiments by XRD.

On the other hand, the results of the temperature-programmed analyses revealed that most of the catalysts were not completely reduced in their activated state. Since the pioneering work of Sabatier and Senderens, metallic Ni is a well-known active component in CO hydrogenation [30]. The results of our analysis suggest that the catalysts in the as-prepared state are present as mixed metal oxides in which the various elements interact strongly with one another. During reduction at elevated temperature, a separation seems to occur, resulting in metallic Ni and the oxidic form of the respective dopant (e.g., Y_2O_3 or HfO_2). It can be deduced that the activated catalyst disposes of small metallic Ni particles, representing the catalytically active components that are separated by small oxidic particles of the dopants. Fig. 12 supports this assumption by showing the XRD patterns of the binary $Hf_9Ni_{91}O_x$ in the as-prepared state (1) as well as after the reaction (2). It is obvious that most of the crystalline Ni oxide was reduced during activation and/or reaction. Broad reflexes in the range of $2\theta = 28$ and 36° indicate the formation of new crystalline parts with small mean particle sizes (approximately 4 and 7 nm) under the reducing conditions. These signals correspond to two oxidic Hf phases (HfO_2: JCPDS 74-1506 and 87-2106). The mean particle size of the crystalline Ni particles in $Hf_9Ni_{91}O_x$ after reaction was 48 nm, which compares well with the 123 nm particle size in activated $Ni_{100}O_x$.

In conclusion, our findings suggest that one major function of the dopants (especially those of the activity-increasing group) is the dispersion and/or stabilization of the catalytically active Ni particles. The question of improved selectivity on the other side remains open. Re was found to drastically change the chemical reactivity as well as the chemoselectivity of the Ni-based catalysts; however, no information on the nature of the Re species has been obtained to date. More detailed examinations are underway to elucidate the influence of the various doping elements on structural properties, as well as the nature of active sites. Furthermore, the requirement of coexisting CO and CO_2 to achieve low CO_2 methanation reactivity as reported previously [17] should be investigated by solo methanation experiments on the materials described herein.

5. Conclusion

Several new and highly selective catalysts have been discovered with the help of HTT. Substrate and chemoselectivity are the domains of enzyme catalysis and use the lock–key principle based on the complementarity of active sites and molecular structures of reagents and products. In inorganic materials, the shape selectivity of zeolites is a general selectivity phenomenon that functions by excluding larger molecules or more bulky structures incapable of penetrating the uniformly narrow zeolite pores. The exceptional selectivity and activity properties of the catalysts reported herein result from as-yet poorly understood and unpredictable effects of the elements used for doping Ni catalysts. We assume that the dispersion of the catalytically active component (Ni) by several dopants is one possible cause of the high activity. The improved selectivity might be based on a modified surface favoring the adsorption of H_2 and CO, while disfavoring CO_2 adsorption. Nevertheless, the exact role and nature of these elements are currently under investigation. It was surprising to find noble metal-free ternary mixed oxides that exhibit unprecedented selectivity to CO hydrogenation in the presence of a large excess of CO_2 through our evolutionary approach. The best catalysts that we discovered are based on Ni, which is useless in undoped form for the reaction of interest. Conventional verification of catalytic performance in academic and industrial laboratories has confirmed high catalytic activity and selectivity at relatively low temperatures of 220–280 °C for $Re_2Y_9Ni_{89}O_x$ and 240–330 °C for $Ti_8Hf_9Ni_{83}O_x$ and a wide temperature range in which CO conversion is exclusively observed (CO_2 conversion <10%). Not only the low starting temperature, but also the operating temperature windows of up to 90 °C, compare well with the temperature window of the reference catalyst of only 30 °C. Conventional tests conducted with realistic reformate feed have shown the initial approach to testing CO and CO_2 hydrogenation in separate HTEs to be valid for this problem. In addition, studies of long-term performance

using HTE have found that the best catalysts show no tendency toward poisoning or deactivation.

References

[1] R.J. Farrauto, Appl. Catal. B 56 (2005) 3.
[2] A. Reiche, S. Haufe, Chem. unserer Zeit 37 (2004) 400.
[3] D.L. Trimm, Appl. Catal. A 296 (2005) 1.
[4] V. Jayaraman, Y.S. Lin, J. Membr. Sci. 104 (1995) 251.
[5] R.J.H. Grisel, B.E. Nieuwenhuys, J. Catal. 199 (2001) 48.
[6] G. Avgouropoulos, T. Ioannides, H.K. Matralis, J. Batista, S. Hocevar, Catal. Lett. 73 (2001) 33.
[7] W.F. Maier, J. Saalfrank, Chem. Eng. Sci. 59 (2004) 4673.
[8] S. Takenaka, T. Shimizu, K. Otsuka, Int. J. Hydrogen Energy 29 (2004) 1065.
[9] M. Echigo, T. Tabata, J. Chem. Eng. Jpn. 37 (2004) 75.
[10] O. Görke, P. Pfeifer, K. Schubert, Catal. Today 110 (2005) 132.
[11] Y. Men, G. Kolb, R. Zapf, V. Hessel, H. Löwe, Catal. Today 125 (2007) 81.
[12] R.A. Dagle, Y. Wang, G.-G. Xia, J.J. Strohm, J. Holladay, D.R. Palo, Appl. Catal. A 326 (2007) 213.
[13] G.A. Mills, F.W. Steffgen, Catal. Rev. 8 (1973) 159.
[14] W.F. Maier, K. Stöwe, S. Sieg, Angew. Chem. Int. Ed. 46 (2007) 6016.
[15] J. Scheidtmann, J.W. Saalfrank, W.F. Maier, Stud. Surf. Sci. Catal. 145 (2003) 13.
[16] G. Frenzer, W.F. Maier, Annu. Rev. Mater. Sci. 36 (2006) 281.
[17] H. Habazaki, M. Yamasaki, B.-P. Zhang, A. Kawashima, S. Kohno, T. Takai, K. Hashimoto, Appl. Catal. A 172 (1998) 131.
[18] N.M. Gupta, K. Ravindranathan Thampi, V.S. Kamble, V.P. Londhe, H. Öz, M. Grätzel, Indian J. Chem. A Inorg. Bio-inorg. Phys., Theor. Anal. Chem. 33 (1994) 365.
[19] S.-I. Fujita, N. Tabezawa, Chem. Eng. J. 68 (1997) 63.
[20] A. Franzen, D. Sanders, J. Scheidtmann, U. Simon, W.F. Maier, QSAR Comb. Sci. 24 (2005) 22.
[21] J.W. Saalfrank, W.F. Maier, Angew. Chem. Int. Ed. 43 (2004) 2028.
[22] C.C. Chen, M.M. Nasrallah, H.U. Anderson, J. Electrochem. Soc. 140 (1993) 3555.
[23] M. Krämer, T. Schmidt, K. Stöwe, F. Müller, H. Natter, W.F. Maier, Appl. Catal. A 302 (2006) 257.
[24] S. Storck, PhD thesis, Universität Essen, 1999.
[25] C. Lettmann, H. Hinrichs, W.F. Maier, Angew. Chem. 117 (2001) 3258.
[26] A. Holzwarth, W.F. Maier, Platinum Met. Rev. 44 (2000) 16.
[27] A. Holzwarth, H.W. Schmidt, W.F. Maier, Angew. Chem. Int. Ed. 37 (1998) 2644.
[28] G. Kirsten, W.F. Maier, in: A. Hagemeyer, P. Strasser, A.F. Volpe (Eds.), High Throughput Screening in Chemical Catalysis, Wiley–VCH, Weinheim, 2004, p. 175.
[29] TOPAS V2.1: General profile and structure analysis software for powder diffraction data, Bruker AXS, Karlsruhe, Germany, 2000.
[30] P. Sabatier, J.B. Senderens, C. R. Hebdomadaires des Seances Acad. Sci. 134 (1902) 689.
[31] H.G.J. Lansink Rotgerink, P.D.L. Mercera, J.G. Van Ommen, J.R.H. Ross, Appl. Catal. 45 (1988) 239.
[32] K.O. Xavier, R. Sreekala, K.K.A. Rashid, K.K.M. Yusuff, B. Sen, Catal. Today 49 (1999) 17.
[33] X.-H. Liu, X.-L. Li, Y. Miao, P.-H. Cao, R.-S. Hu, Y.-Q. Ding, J. Nat. Gas Chem. 3 (1994) 468.
[34] R.D. Shannon, Acta Crystallogr. A 32 (1976) 751–767.